12 Application of Fission-Track Thermochronology to Understand Fault Zones

Takahiro Tagami

Abstract

The timing and thermal effects of fault motions can be constrained by fission-track (FT) thermochronology and other thermochronological analyses of fault zone rocks. Materials suitable for such analyses are produced by fault zone processes, such as: (1) mechanical fragmentation of host rocks, grain-size reduction of fragments and recrystallisation of grains to form mica and clay minerals, (2) secondary heating/melting of host rocks as the result of friction and (3) mineral vein formation as a consequence of fluid flow associated with fault motion. The geothermal structure of fault zones is primarily controlled by three factors: (a) the regional geothermal structure around the fault zone that reflects the background thermotectonic history of the study area, (b) frictional heating of wall rocks by fault motion and consequent heat transfer into surrounding rocks and (c) thermal effects of hot fluid flow in and around the fault zone. The thermal sensitivity of FTs is briefly reviewed, with a particular focus on the fault zone thermal processes, i.e., flash and hydrothermal heating. Based on these factors, representative examples as well as key issues, including sampling strategy, are highlighted for using thermochronology to analyse fault zone materials, such as fault gouges, pseudotachylytes and mylonites. The thermochronologic analyses of the Nojima fault in Japan are summarised, as an example of multidisciplinary investigations of an active seismogenic fault system. Geological, geomorphological and seismological implications of these studies are also discussed.

12.1 Introduction

Seismic activity and faulting are manifestations of geodynamic processes of the dynamic Earth. They involve a series of fault zone processes and products, such as gouge and pseudotachylyte formation, as a result of repeated fault motions on a geologic timescale at different crustal depths. Because those processes are accompanied by temperature changes along the fault zone, geo- and thermochronological techniques are potentially useful to detect and date the thermal episodes under active and ancient faulting regimes. In particular, fission-track (FT), K–Ar (Ar/Ar) and U–Th methods have successfully been applied to fault zone rocks at a variety of tectonic settings (e.g. Flotte et al. 2001; van der Pluijm et al. 2001; Mulch et al. 2002; Boles et al. 2004; Murakami and Tagami 2004; Sherlock et al. 2004; Zwingmann and Mancktelow 2004; Murakami et al. 2006a; Rolland et al. 2007; Haines and van der Pluijm 2008; see Tagami 2012 for a review). In addition, (U–Th)/He analyses have recently been conducted on zircon separates from fault zones (Yamada et al. 2012; Maino et al. 2015; see also Ault et al. 2015 for haematite analysis).

Compared to other techniques, the advantages of the FT (and also the (U–Th)/He) method where applied to fault zones are: (1) greater thermal sensitivity for secondary heating episodes associated with faulting; (2) higher mechanical/chemical survivability of mineral grains used for FT analysis (e.g. zircon) in the core of fault zones and (3) widespread occurrence of mineral grains used for FT analysis (i.e. apatite and zircon) within continental crust rocks. As a result, FT analysis revealed thermal histories in or near fault zones in various regions, for example, the Median Tectonic Line in Japan (Tagami et al. 1988), the Alpine fault in New Zealand (Kamp et al. 1989), the Pejo fault system in the Italian Eastern Alps (Viola et al. 2003), the San Gabriel Fault in California (d'Alessio et al. 2003) and the Nojima Fault in Japan (Murakami and Tagami 2004).

T. Tagami (✉)
Division of Earth and Planetary Sciences, Kyoto University, 606-8502 Kyoto, Japan
e-mail: tagami@kueps.kyoto-u.ac.jp

M. G. Malusà and P. G. Fitzgerald (eds.), *Fission-Track Thermochronology and its Application to Geology*,
Springer Textbooks in Earth Sciences, Geography and Environment, https://doi.org/10.1007/978-3-319-89421-8_12

This chapter reviews the state-of-the-art of FT thermochronology of seismogenic fault zones and illustrates the relevant scientific backgrounds of fault zone processes and materials, geothermal regime of fault zones, thermal stability of FTs in fault settings and key studies of application to different fault lithologies.

12.2 Fault Zone Processes and Materials

12.2.1 Faults and Fault Zone Rocks

The schematic cross-section of a typical fault zone[1] is shown in Fig. 12.1a, where the geologic features of fault rocks are presented along with thermomechanical characteristics (see also Chap. 10, Malusà and Fitzgerald 2018). Fault zone rocks are classified as gouges, cataclasites, pseudotachylytes, mylonites, etc., based primarily on their textures (Sibson 1977). The formation process of fault zone materials includes three primary categories: (1) mechanical fragmentation of host rocks, coupled with grain-size reduction and recrystallisation to form secondary minerals, such as clay; (2) frictional heating by fault motions that occasionally leads to melting of wall rocks and (3) fluid flow and chemical precipitation to form mineral veins. These processes are described below in more detail.

12.2.2 Grain-Size Reduction and Recrystallisation

Frictional fault motion, which is controlled by brittle fracture at shallow crustal levels, causes damage and abrasion of host-rock surfaces. As a result, loose particles with angular shapes, called gouge, are formed. As the faulting progresses, the gouge shears as a granular material, resulting in a systematic reduction in the average grain size.

Fault gouges generally contain a variety of neoformed clay minerals, such as illite and smectite. In igneous and metamorphic environments, in situ clay mineralisation plays a major role in forming authigenic clays in gouge. Fluid flow is likely a key factor to promote mineralogical reactions, and the authigenic illites formed are useful for K–Ar (Ar/Ar) dating.

At deeper crustal levels where rock-forming minerals are semi-brittle to plastic, ductile faulting (or shearing) is dominant and likely forms mylonites. Recrystallisation of biotite takes place at ~350–400 °C (Simpson 1985), whereas white micas are formed by synkinematic crystallisation at the expense of feldspars at ~400 °C (Rolland et al. 2007). Those newly formed micas are widely used for Ar/Ar thermochronology (see Tagami 2012 for more details).

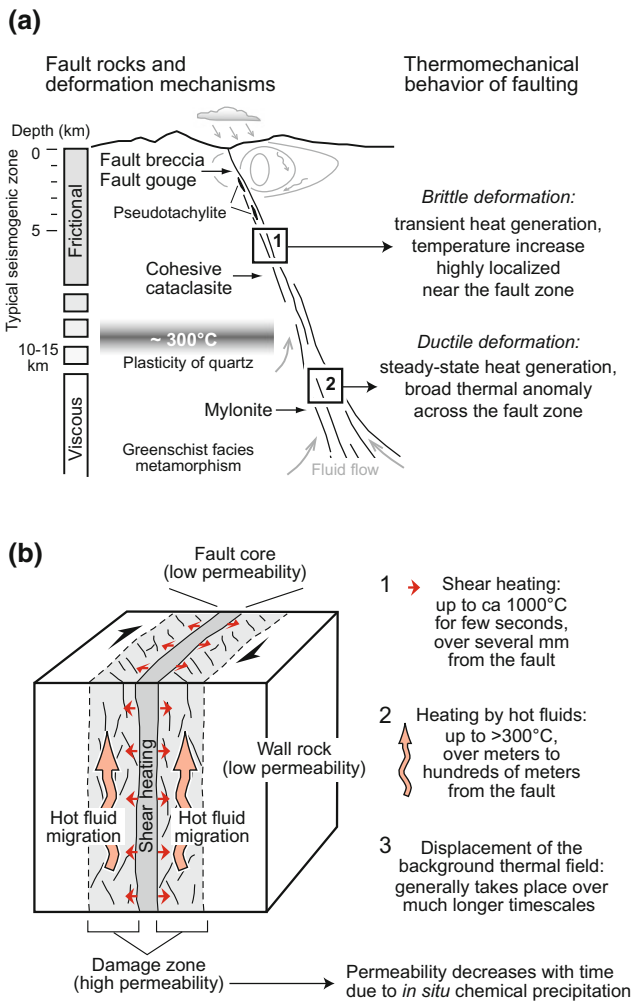

Fig. 12.1 Synoptic model of a fault zone. **a** Fault rocks and deformation mechanisms against depth (and temperature). **b** Permeability structure and thermal regime (after Scholz 1988; Tagami 2012, as modified from Fig. 10.4a—Malusà and Fitzgerald 2018)

12.2.3 Frictional Heating and Pseudotachylyte Formation

The mechanical work of faulting primarily comprises three factors: (a) frictional heating, (b) surface energy of gouge formation and (c) elastic radiation (Scholz 2002). Factors (b) and (c) are in general much less important than frictional heating, and thus the mechanical work is primarily expended by the generation of frictional heat. The generation of heat on a fault plane can accordingly be approximated as:

$$\tau v = q \tag{12.1}$$

[1]"Fault zone" is a term to describe the spatial extent along a fault where rocks are significantly deformed by the faulting.

where τ is the mean shear stress acting on a fault sliding at velocity v, and q is the heat flow generated by the fault motion (Scholz 2002).

The thermomechanical behaviour of faulting is classified into two general regimes: (a) under brittle conditions, a transient heat pulse is generated by rapid coseismic fault slip, with $v = \sim 10–100$ cm/s; (b) under ductile conditions, heat generation can be regarded as steady-state, due to a long-term fault motion averaged over geological time, with $v = \sim 1–10$ cm/year (Scholz 2002).

In the brittle regime, heat generation is highly localised near the fault zone owing to the greater v coupled with low thermal conductivity of rocks. In this case, fault zone rocks can occasionally be molten to form glassy vein-shaped rocks, called pseudotachylytes (Sibson 1975). In contrast, the latter type of heating is expected to form a broader, regional thermal anomaly across the fault zone due to the smaller v and constant heat generation. Some regional metamorphic aureoles in convergent plate boundaries (or transcurrent shear zones) may be attributable to such long-term heating at depths (Scholz 1980). In both regimes, the time and magnitude of heating can be assessed quantitatively by thermochronology using FT and other techniques, although the rock sampling strategy is substantially different between the two.

The energy budget of earthquakes can also be estimated by thermochronological methods. The mechanical work of fault motion, W_f, is a function of mean shear stress, which is difficult to measure directly on the fault plane. Thus, an available approach to constrain W_f is to measure the generated heat flow q during an earthquake. This can be achieved either by: (a) detection of the temperature anomaly across the fault zone by drilling into the fault soon after the earthquake (Brodsky et al. 2010, and references therein), or (b) geothermometric analyses of fault zone rocks that experienced frictional heating, such as vitrinite reflectance or FT analysis (e.g. O'Hara 2004).

12.2.4 Fluid Flow and Mineral Vein Formation

A variety of mineral veins in fault zones, such as calcite, quartz and ore deposits, are typically formed as fracture fillings under an extensional regime, as a consequence of fluid flow and in situ chemical precipitation. At crustal temperatures exceeding 200–300 °C, the healing and sealing of fractures effectively proceeds to produce veins, probably within the conventional lifetime of hydrothermal systems (Cox 2005). Hence, the formation of extensional vein arrays in seismogenic crustal depths can closely represent the time of brittle failure and permeability enhancement that induce fluid flow. During the seismic cycle of a fault system, a significant slip event likely produces large ruptures in the fault zone, reduces the fault strength, enhances fluid flow and eventually leads to veins formation (e.g., Sibson 1992). This seismic episode is followed by an interseismic period when the fault strength is progressively recovered as the healing and sealing of ruptures progresses. This evolution is called fault-valve behaviour (Sibson 1992).

The time of brittle failure and permeability enhancement of a fault zone can be constrained by dating mineral veins. U–Th disequilibrium analysis of carbonate veins has successfully been applied to date neo-tectonic fault systems (Flotte et al. 2001; Boles et al. 2004; Verhaert et al. 2004; Watanabe et al. 2008; Nuriel et al. 2012). In addition, hot fluid flow caused by brittle faulting should be recorded in adjacent wall rocks as a thermal anomaly, which may be detected by low-temperature thermochronology of host minerals, e.g. FT analysis on apatite and zircon separated from fault zone rocks.

12.3 Thermal Regime of Fault Zones

This section provides a brief overview of temperature variations in a fault zone in space and time. The thermal regime is a key parameter governing the response of applied thermochronometers in terms of thermal stability (or retentivity/diffusivity) of accumulated daughter nuclides (or lattice damages) in the target mineral.

12.3.1 Regional Geothermal Structure and Background Thermal History

The geothermal structure of solid Earth can be approximated by a one-dimensional temperature profile against depth from the Earth's surface. The temperature increases toward the centre of the Earth, with a higher geothermal gradient within the lithosphere. Tectonics perturbs the first-order geothermal structure of the upper continental crust with significant departures from its average geothermal gradients, generally assumed to be on the order of 30 °C/km (see discussion in Chap. 8, Malusà and Fitzgerald 2018). The thermal regime of a fault zone is controlled by three factors (Fig. 12.1b): (a) the regional geothermal structure and background thermal history of the study area, (b) frictional heating of the wall rocks during faulting in the brittle regime and (c) heating of the wall rocks by hot fluid flow in and around the fault zone.

Where the fault motion has some vertical component, the two blocks separated by the fault show differential uplift/subsidence movements with respect to each other. If uplift is accompanied by exhumation, the rocks within the

uplifted block effectively cool down, due to the resultant long-term downward motion of geotherms to adjust for the new state of geothermal equilibrium. Conversely, if subsidence is accompanied by sediment deposition, the rocks within the subsided block are effectively heated, as a result of burial and long-term upward motion of geotherms (note that the thermal effects of thrust faulting can be grossly different (e.g. Metcalf et al. 2009)). As the fault motion continues, the amount of fault slip accumulates and thus the difference in the thermal signature progressively increases between rocks that were once juxtaposed each other across the fault boundary. The difference eventually may become large enough to be resolved by an appropriate thermochronometric technique, which then places constraints on the timing and magnitude of vertical components of the accumulated fault motions. Low-temperature thermochronology using (U–Th)/He, FT and/or K–Ar (^{40}Ar/^{39}Ar) techniques is particularly useful for reconstructing such regional thermal histories. Note that such modifications to the background thermal structure occur over timescales that are much longer than those characterising thermal processes within a fault zone, i.e. frictional heating in the brittle regime and hot fluid flow. Also note that, on a regional scale, the background thermal history may vary depending on a variety of factors, such as surface topography, spatial variation of geothermal structure, tectonic tilting and ductile deformation at depth (see Chap. 8, Malusà and Fitzgerald 2018).

12.3.2 Frictional Heating of Wall Rocks by Fault Motion

Frictional heating in the brittle deformation regime is characterised by episodic temperature increase up to ~1000 °C, within a typical time period of several seconds and a spatial range of several mm from the fault (Fig. 11.1b). Lachenbruch (1986) quantified the production of frictional heat and its conductive transfer into wall rocks, using the heat conduction models of Carslaw and Jaeger (1959). Suppose a fault slips along a fault zone of width $2a$ during a time interval $0 < t < t^*$, where t^* is a duration of the slip. Within the fault zone ($0 < x < a$, where x is a distance to the fault plane), the temperature rise ΔT during faulting ($t < t^*$) is given by

$$\Delta T = \frac{\tau}{\rho c}\frac{v}{a}\left\{t\left[1 - 2\iint erfc\frac{a-x}{\sqrt{4\alpha t}} - 2\iint erfc\frac{a+x}{\sqrt{4\alpha t}}\right]\right\} \tag{12.2}$$

where ρ is the density, c is the specific heat and α is the thermal diffusivity (Fig. 12.2), whereas the temperature rise after faulting ($t^* < t$) is given by

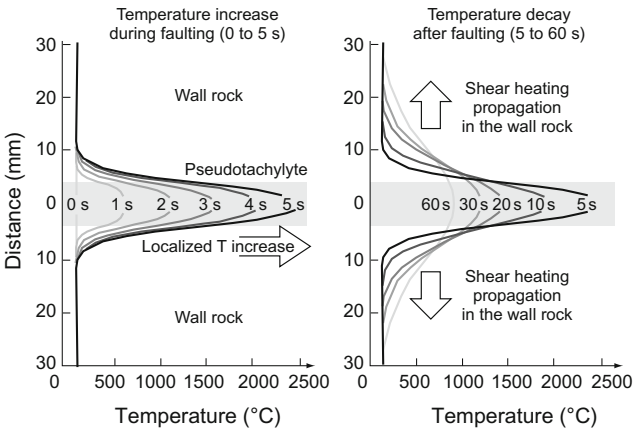

Fig. 12.2 Profiles of temperature increase during faulting (left) and temperature decay after a faulting event (right), for a shear work of 50 MPa m. The temperature increase ΔT was calculated using the equations of Carslaw and Jaeger (1959) and Lachenbruch (1986), assuming a duration of the local seismic slip of 5 s. The temperature exceeds 1000 °C in a faulting zone of 8 mm width (grey box) for ~30 s, following the onset of faulting (after Murakami 2010)

$$\Delta T = \frac{\tau}{\rho c}\frac{v}{a}\left\{t\left[1 - 2\iint erfc\frac{a-x}{\sqrt{4\alpha t}} - 2\iint erfc\frac{a+x}{\sqrt{4\alpha t}}\right] - (t-t^*)\left[1 - 2\iint erfc\frac{a-x}{\sqrt{4\alpha(t-t^*)}} - 2\iint erfc\frac{a+x}{\sqrt{4\alpha(t-t^*)}}\right]\right\} \tag{12.3}$$

Instead, outside of the fault zone ($x > a$), the temperature rise ΔT during faulting ($t < t^*$) is given by

$$\Delta T = \frac{2\tau}{\rho c}\frac{v}{a}\left\{t\left[\iint erfc\frac{x-a}{\sqrt{4\alpha(t)}} - \iint erfc\frac{x+a}{\sqrt{4\alpha(t)}}\right]\right\} \tag{12.4}$$

and the temperature elevation after faulting ($t^* < t$) is given by

$$\Delta T = \frac{2\tau}{\rho c}\frac{v}{a}\left\{t\left[\iint erfc\frac{x-a}{\sqrt{4\alpha t}} - \iint erfc\frac{x+a}{\sqrt{4\alpha t}}\right] - (t-t^*)\left[\iint erfc\frac{x-a}{\sqrt{4\alpha(t-t^*)}} - \iint erfc\frac{x+a}{\sqrt{4\alpha(t-t^*)}}\right]\right\} \tag{12.5}$$

The mean shear stress τ can then be estimated using these equations, where geothermometric analysis of known kinetics is carried out (O'Hara 2004; Tagami 2012).

According to Lachenbruch (1986), if the slip duration t^* is negligibly small relative to post-seismic observation time ($t - t^*$), and also if our observation time t is sufficiently large compared to the time constant λ of the shear zone ($\lambda = a^2/4\alpha$), Eqs. (12.2)–(12.5) can be simplified (for any x, $t \gg t^*$, and $t \gg \lambda$) to

$$\Delta T = (\tau u/\rho c)\,(\pi\alpha t)^{-1/2} \exp\left(-x^2/4\alpha t\right) \tag{12.6}$$

where u is the slip distance ($u = vt^*$). The mean shear stress τ can accordingly be calculated for certain x and t conditions by substituting individual appropriate values to ρ, c and α, and by measuring ΔT and u. This approach was applied to the case of temperature anomaly measurement across a fault zone, conducted by drilling into the fault soon after the earthquake (Brodsky et al. 2010).

12.3.3 Hot Fluid Flow in and Around the Fault Zone

Fluid flow within a fault zone can be inferred from the occurrence of mineral veins formed by in situ chemical precipitation (see Sect. 12.2.4). The spatial range of the effective flow is primarily on the order of 1–100 m normal to the fault, based on natural occurrences of mineral veins (e.g. Boles et al. 2004; Watanabe et al. 2008; Cox 2010). The permeability structure of fault zones, which is a key to control the flow, in general consists of three regions: (a) the fault core, which comprises fault gouge and breccia, both characterised by low permeability; (b) the damage zone, which consists of fractured rocks and has high permeability that offers effective pathways for seepage flows and (c) the bedrock protolith with low permeability (Evans et al. 1997; Seront et al. 1998). The mean permeability of a fault zone is inferred to decrease with time, as a result of narrowing/closure of pathways due to the continued fluid flow with chemical precipitation to form veins. The permeability likely recovers if the fault zone experiences new seismic activity and resultant reopening of the pathways. This temporal model was first tested by the Nojima Fault Zone Probe Project (see review in Tagami 2012).

If the seepage flow in a fault zone is dominated by upward components, the fault zone is heated by flows from deeper crustal levels and is hotter than the environmental temperature (Fig. 12.1b). Hot springs are often found near active fault systems, and some of them likely have deep origins as indicated by their geochemical signatures (e.g., Fujimoto et al. 2007). Some of the large faults continue from the surface to >10 km depths (Scholz 2002), and the temperature of upcoming fluids is estimated to exceed 300 °C under the assumption of a normal geothermal gradient of ~30 °C/km, and neglecting heat loss during seepage flow.

12.4 FT Stability During Flash and Hydrothermal Heating

This section gives a brief overview of the kinetic formulation of FT annealing and its application to fault zone settings. If a host rock undergoes a temperature increase, fission tracks that have been accumulated are shortened progressively and eventually erased by thermal annealing. The reduction of FT lengths is a function of heating time and temperature, and the temperature interval of partial annealing is substantially variable among different minerals. FT annealing is more precisely quantified by using the reduction of etched track length than the etched track density (see Chap. 3, Ketcham 2018), and the shape of the track-length distribution is diagnostic of the thermal history of the rock. Accordingly, horizontal confined track lengths are routinely analysed to determine the annealing kinetic functions, an example of which is:

$$\mu = 11.35\left[1 - \exp\left\{-6.502 + 0.1431\,\frac{(\ln t + 23.515)}{(1000/T - 0.4459)}\right\}\right] \tag{12.7}$$

where μ is the mean FT length in zircon, after annealing at T Kelvin for t hours (Tagami et al. 1998). For more details, see other comprehensive reviews (e.g. Donelick et al. 2005; Tagami 2005; Tagami and O'Sullivan 2005).

The thermal regime of fault zones is characterised by frictional heating and hot fluid flow, in addition to the regional background geothermal structure. Hence, for reliable FT thermochronologic analysis of fault zones, additional consideration is needed to assess the influence of both high-temperature short-term heating and hydrothermal heating on the FT annealing kinetics (which is usually determined in a dry atmospheric environment in a conventional laboratory and extrapolated to geological timescales).

Laboratory heating experiments to simulate thermal perturbations at hydrothermally pressurised conditions due to hot fluid flow were performed on zircon (Brix et al. 2002; Yamada et al. 2003) using a hydrothermal synthetic apparatus. It was found using the same zircon sample and analytical procedure that the observed FT length reduction in the atmosphere is indistinguishable from that under hydrothermal conditions (Yamada et al. 2003). The results of Brix et al. (2002) using Fish Canyon Tuff zircon also exhibit consistency of annealing kinetics between dry and hydrothermal conditions. It thus suggests that the conventional zircon annealing kinetics can also be applied to hydrothermal heating conditions in nature, such as fault zones and sedimentary basins settings.

Frictional heating along a fault in the brittle regime is a short-term geological phenomenon with an effective heating duration on the order of seconds, which is significantly

shorter than the conventional laboratory heating of $\sim 10^{-1}$ to 10^4 h. Thus, high-temperature and short-term heating (i.e. flash heating) experiments were specially designed and conducted using a graphite furnace coupled with infrared radiation thermometers (Murakami et al. 2006b). The observed track-length reduction in zircon by 3.6–10 s of heating at 599–912 °C is, overall, slightly greater than that predicted by the zircon FT annealing kinetics, based upon the heating for $\sim 10^{-1}$ to 10^4 h at ~350–750 °C (Yamada et al. 1995; Tagami et al. 1998). Yamada et al. (2007) proposed revised kinetic models that integrate results of both the flash heating and conventional laboratory to geological heating. It should be noted here that spontaneous tracks in zircon are totally annealed at 850 ± 50 °C for ~4 s, suggesting that the zircon FT system can be completely reset during the ordinary pseudotachylyte formation in nature (Otsuki et al. 2003).

A note should be added concerning FT annealing kinetics of apatite. The kinetics has been established in dry atmospheric environments in conventional laboratories and also tested and calibrated on geological timescales by analysing drilled cores of sedimentary basins. However, the influences of both flash and hydrothermal heating on the kinetics are not well known yet, and thus specially designed experiments are strongly needed for apatite. These experiments will provide a more robust basis for interpreting apatite FT data in terms of frictional heating and hot fluid flow in fault zones.

12.5 Rock Sampling Strategy

The rock sampling strategy for fault zone studies may be different from other applications primarily due to the characteristic heat source associated with faulting in the brittle regime (cf. Chap. 10, Malusà and Fitzgerald 2018, and Chap. 11, Foster 2018). As argued above, three thermal factors relevant to the fault zone generally yield characteristic thermal histories (i.e. temperature–time paths) with different spatial ranges (Fig. 12.1b): (a) background thermal history that reflects long-term tectonics of crustal basement, with an ordinary spatial range of ~1–100 km from the fault; (b) episodic frictional heating up to an order of 1000 °C (i.e., occasionally above the melting temperature of wall rocks), with a typical time period of several seconds and spatial range of several mm from the fault (in case of brittle deformation) and (c) heating by hot fluid flow, with temperatures below the melting point of host rock, within ~100 m of the fault zone. In theory, we can place constraints on each of these three factors by analysing a series of rocks in and around the fault zone using thermochronological techniques. In planning the research strategy toward this goal, we need to take into account the following geological and analytical aspects:

- First of all, we need to choose appropriate thermochronometers with thermal sensitivities suited to the expected temperature and time ranges of the thermal history of interest.
- If we want to analyse heating events localised to the fault zone, i.e. factors (b) and (c), the background thermal history of the protolith needs to be simple, so that we can readily extract the thermal history signals of interest from the background noise. In addition, the background thermal history needs to be the same along the fault; otherwise, each locality chosen for analysis will have different boundary conditions.
- To conduct thermochronologic analysis with good resolution, it is also desirable to have a large age contrast between the background thermal history and the heating event(s) of the fault zone.
- In order to reveal localised heating events, it is essential to choose the optimal traverse(s) across the fault zone that will satisfy the above conditions. Hence, adequate knowledge is required also on the spatial geometry of the fault plane.

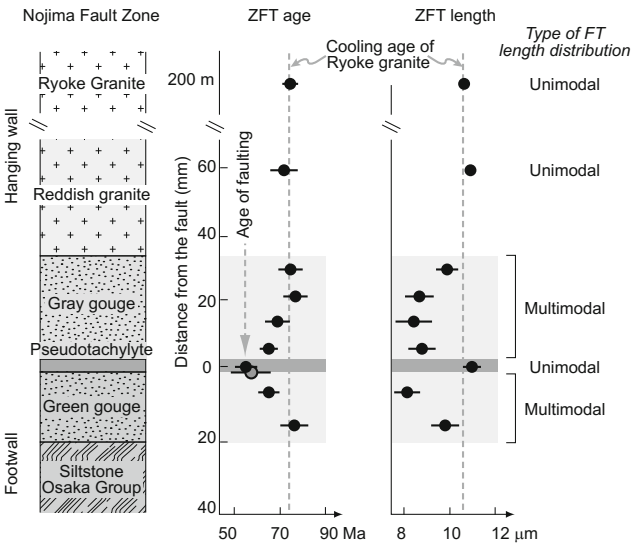

Fig. 12.3 Lithology of the sampled fault rock section in the Hirabayashi trench of the Nojima Fault, Japan, along with a plot of mean age, mean length and type of length distributions of fission tracks in zircon (ZFT). Another sample from the pseudotachylyte layer is also plotted (grey circle). The grey-dashed lines represent the mean age and length of a sample from the Ryoke host rock collected at ~200 m away from the fault. The sample from the pseudotachylyte layer has an age significantly younger than that of initial cooling of the samples from the Ryoke host rock. Error bars are ±1 SE (after Murakami and Tagami 2004)

To constrain the three factors (a)–(c) with good confidence, we need to collect rock samples at different spatial intervals toward the fault plane. At localities >100 m distant from the fault, the interval is not necessarily short and thus rocks can be sampled as for ordinary thermochronologic studies. As approaching the fault, however, we need to make the sample interval shorter in order to determine the possible spatial change of thermochronologic data. In particular, where we intend to detect the thermal effects of the factor (b) (i.e. frictional heating), the interval should be kept as short as several mm within ~10 cm of the fault plane (d'Alessio et al. 2003; Murakami and Tagami 2004) (Figs. 12.3 and 12.4). Such rock sampling requires a special caution for handling brittle fault rocks, such as cataclasites and mylonites. If possible, the section across the fault plane could be cut into blocks by a portable rock saw, so that the sample blocks can be brought back to the laboratory for precise and contamination-free sampling (e.g. manual cutting by metal blades, handpicking pieces by tweezers). Otherwise, fault rocks need to be precisely divided and sampled in situ, with special care to avoid possible contamination. In these regards, the ideal condition may be to sample rocks from a continuous drill core section across the fault. Alternatively, trenching the fault will offer an opportunity to sample fault zone rocks in a three-dimensional geometry. In contrast, the sampling strategy for fault zones in the ductile regime is substantially different from that of the brittle regime mentioned above. This is because the expected heat generation in the ductile regime is steady state over geological time, with a faulting velocity of ~1–10 cm/year (see Sect. 12.2.3), and this likely results in a broader, regional thermal anomaly across the fault zone. As will be documented in Sect. 12.6.2, the spatial extent of the thermal anomaly may reach 10 km away from the fault. Hence, the spatial interval between individual rock sampling localities need not be short, as for sampling within the brittle regime, and thus rocks can be sampled as the ordinary thermochronologic studies. It is noted, however, that the thermal anomaly formed by ductile faulting may be difficult to distinguish from the background thermal history using thermochronology, because the two thermal processes may lead to similar spatial distributions of thermochronologic data.

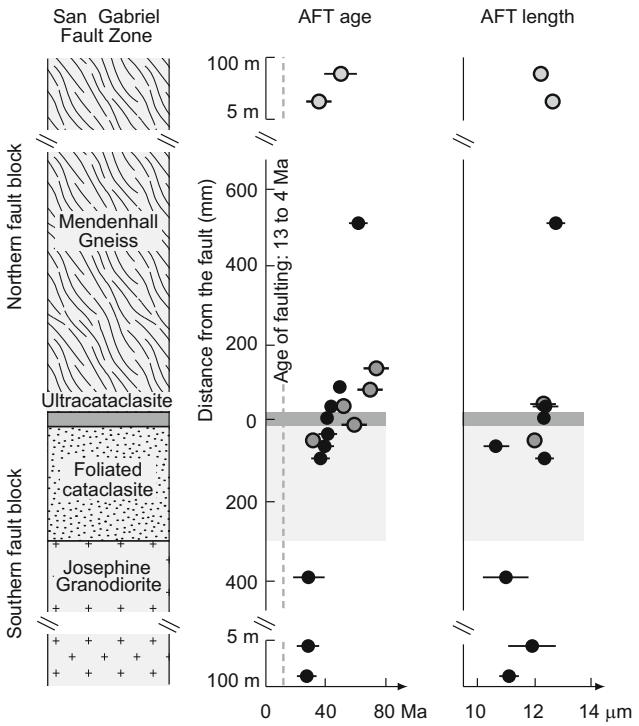

Fig. 12.4 Lithology of the sampled fault rock section of the San Gabriel fault zone, southern California, along with a plot of mean age and length of fission tracks in apatite (AFT). Data from two transects across the fault are shown in different symbols, neither of which show any significant reductions by the fault activity, even in samples within just 2 cm of the ultracataclasite. Error bars are ±1 SE uncertainty (after d'Alessio et al. 2003)

12.6 Key Studies

12.6.1 The Nojima Fault

The Nojima Fault runs along the northwestern coast of the Awaji Island, Hyogo Prefecture, Japan and is a high-angle reverse fault dipping 83° SE with a right-lateral slip component. A >10 km long surface rupture was formed along the active Nojima Fault, as a result of the 1995 Kobe earthquake (Hyogoken-Nanbu earthquake; M7.2). Shortly after the earthquake, the Nojima Fault Zone Probe Project was initiated as a multidisciplinary geoscience program (Oshiman et al. 2001; Shimamoto et al. 2001; Tanaka et al. 2007), involving drilling a series of boreholes that penetrated the fault at depth. Two boreholes penetrated the Nojima Fault at different depths with nearly complete core recoveries: at 625.27 m by the Geological Survey of Japan 750 m (GSJ-750) borehole at the Hirabayashi (northern) site; and at 389.4 m by the University Group 500 m (UG-500) borehole at the Toshima (southern) site. In addition, the Nojima Fault was also trenched at Hirabayashi, where the fault rocks exposed include, from the hanging wall to the footwall, a granitic cataclasite, a 2–10 mm wide pseudotachylyte layer and the siltstone of the Osaka Group. At Hirabayashi, the fault rupture formed in 1995 is located about 10 cm below the pseudotachylyte.

Using the Hirabayashi trench, Murakami and Tagami (2004) carried out FT analysis on zircon separates from a 50-cm-wide grey fault rock that, from the footwall toward the hanging wall, consists of (1) greenish-grey gouge of the footwall (NT-LG; ~20 mm wide), (2) pseudotachylyte

(NT-Pta; ~2–10 mm wide), (3) grey gouge of the hanging wall (NT-UG; ~30 mm wide) and (4) reddish granite (NF-HB1; ~20 mm wide) (Fig. 12.3). Otsuki et al. (2003) estimated the temperature of the pseudotachylyte formation as ~750–1280 °C, based primarily on the observation of melting of K-feldspar and plagioclase. Both FT ages and track lengths systematically vary with distance to the pseudotachylyte, with the youngest age of 56 ± 4 (1SE) Ma from the pseudotachylyte layer. While the age of background regional cooling is 74 ± 3 Ma, four gouge samples from the hanging wall (i.e. NT-UG 1–4) and two gouge samples from the footwall yielded ages of 65–76 Ma, with progressive younging toward the pseudotachylyte. The track-length distribution changes when approaching the pseudotachylyte from unimodal (long tracks) to widespread multimodal (long and short tracks), and eventually to unimodal again (long tracks). These data suggest that the zircon FT system in the pseudotachylyte layer was totally reset and subsequently cooled at ~56 Ma, with a thermal perturbation occurring in the surrounding fault zone rocks. This interpretation is supported by a combination of (a) the temperature estimate for the Nojima pseudotachylyte formation of ~750–1280 °C, on the basis of feldspar melting textures (Otsuki et al. 2003) and (b) laboratory flash heating experiments of zircon FT system (Murakami et al. 2006b).

The borehole rocks from GSJ-750 and UG-500 were also analysed by zircon FT thermochronology (Tagami et al. 2001; Murakami et al. 2002; Tagami and Murakami 2007). Zircon age and length data suggest: (a) an ancient heating event causing a temperature increase into the zircon partial annealing zone (PAZ) within ~25 m in both the footwall and hanging wall at the Hirabayashi borehole (GSJ-750) and (b) an ancient heating into the zircon PAZ within 3 m of the fault in the hanging wall only at Toshima (UG-500). The age of the last cooling after the secondary heating was estimated on partially annealed samples near the fault using the Monte Trax inverse modelling (Gallagher 1995) as 35.0 ± 1.1 (1SE), 38.1 ± 1.7 and 31.3 ± 1.4 Ma at the Hirabayashi borehole (GSJ-750), and 4.4 ± 0.3 Ma at Toshima (UG-500). The maximum temperature experienced during the secondary heating is not uniquely determined since the degree of FT annealing also depends on the heating duration. The source of the secondary heating is likely heat transfer and dispersion via fluids within the fault zone because the spatial range of the annealing zone (i.e. ~25 m and ~3 m from the fault) is too large to be attributed to simple heat conduction. This interpretation is also favoured by the fact that the degree of FT annealing is positively correlated with deformation/alteration of the borehole rocks. The result of the in situ heat dispersion calculation indicates that in situ frictional heat is not sufficient to explain the degree of FT annealing, and hence some additional heat is required, for example, upward flow of hot fluid along the fault zone from deeper crustal levels.

Zwingmann et al. (2010a) reported authigenic illite K–Ar ages from six granitic samples outcropping at Hirabayashi, including three fault gouge samples in close proximity to the pseudotachylyte layer. The six ages of the <2 μm fractions fall in the range of 56.8 ± 1.5 (1SE) to 42.2 ± 1.0 Ma, whereas the <0.1 and <0.4 μm fractions of the three gouge samples are anomalously younger at 30.3 ± 0.9 to 9.1 ± 1.6 Ma. The former ages (57–42 Ma) are younger than the time of regional cooling of the granitic protolith (74 ± 3 Ma) and interpreted as the time of brittle faulting. The latter ages (30–9 Ma) on the finer fractions, which have lower effective closure temperatures, probably reflect a secondary loss of radiogenic ^{40}Ar, likely as a result of thermal overprints near the fault caused by hot fluid flow. Five UG-500 core samples were also analysed at Toshima, with three ages from 50.7 ± 1.2 to 45.0 ± 0.9 Ma for the <0.4 and <2 μm fractions (less K-feldspar contamination), suggesting a time of brittle faulting similar to that of the Hirabayashi outcrop.

In addition, Watanabe et al. (2008) measured U–Th radioactive disequilibrium on calcite veins from 1484 m depth from the UG-1800 m borehole at Toshima (~1 km southwest of the UG-500 drilling locality). The presence of radioactive disequilibrium in $^{234}U/^{238}U$ suggests that the age of calcite precipitation was younger than 1 Ma, which constrains the time of fluid infiltration into the fault zone. Furthermore, electron spin resonance (ESR) analyses conducted on borehole rocks from the UG-500, documented that the ESR intensity (Al and E′ centres) is significantly reduced within ~3 mm from the fault plane (Fukuchi and Imai 2001; Matsumoto et al. 2001). This is likely caused by frictional heating of the Nojima Fault, suggesting that the ESR method can potentially be applied to dating recent movements of an active fault system.

Based on the thermochronologic and other constraints mentioned above, a plausible evolution for the Nojima Fault is reconstructed as follows (see Tagami and Murakami (2007) and Zwingmann et al. (2010a) for more details):

- By ~56 Ma, the fault had already initiated as an in-plane fault offset at crustal depths. The depth may have been >15 km based on fluid inclusion data (Boullier et al. 2001).
- From ~56 to 42 Ma, brittle faulting took place (or had continued) in some of the segments of the ancient Nojima fault.
- At ~35 and 4 Ma at Hirabayashi and Toshima, respectively, fault activity was accompanied by heat transfer and dispersion via fluids circulating within the fault zone.

- At ~1.2 Ma, the present Nojima fault system was formed by the reactivation of the ancient Nojima Fault. Note that such reactivation phenomena have been widely recognised elsewhere (e.g. Holdsworth et al. 1997).

Another important tectonic constraint derived from zircon FT data of the Nojima pseudotachylyte is that the mean shear stress τ can be estimated by combining Eqs. (12.2) to (12.5) of frictional heat production and conductive transfer and Eq. (12.7) of zircon FT annealing (Murakami 2010). The logic of this approach is:

- Temperature profiles are given through time t for a specific τ by assigning or assuming parameters of Eqs. (12.2) to (12.5), i.e. the density ρ, specific heat c, thermal diffusivity α, fault zone width a, sliding velocity v and slip duration t^*.
- The thermal history at each locality can be derived from the series of temperature profiles above, by specifying a certain distance from the fault centre, x.
- For a certain combination of τ and x values, a mean FT length μ is predicted using Eq. (12.7), by integrating the annealing effects for each of the divided time intervals of the thermal history.
- Accordingly, for a certain τ value, a spatial profile of predicted μ is constructed against x.
- For a range of τ values, the spatial profiles of μ are computed and compared with measured FT length data, in order to search for the best fitting τ value.

Consequently, the net shear work (i.e. $\tau v t^*$) was estimated as ~50 MPa m for the faulting event at ~56 Ma (Murakami 2010), which likely favours the "strong" fault model that supports higher shear stresses (Scholz 2002).

12.6.2 Other Examples

Fault Gouges Although fault gouges are widespread along fault cores in most active fault systems, the application of the FT techniques to these rocks is quite limited and has not been very successful in constraining the areal extent of thermal perturbation or the age of faulting. D'Alessio et al. (2003) conducted apatite FT analysis on the samples adjacent to and within the San Gabriel fault zone, southern California, which was likely active from 13 to 4 Ma and has since been exhumed from depths of 2 to 5 km. At the studied locality, the San Gabriel fault consists of an ultracataclasite zone of 1–8 cm width that juxtaposes the Medenhall gneiss to the north with the Josephine granodiorite to the south (Fig. 12.4). Apatite FT ages and lengths show no significant reductions by the fault activity, even in samples within just 2 cm from the ultracataclasite. The absence of any measurable FT annealing implies that either each slip was never larger than 4 m, or the average apparent coefficient of friction was <0.4, on the basis of the forward modelling of heat generation, heat transport and apatite FT annealing.

Wolfler et al. (2010) applied the apatite FT and (U–Th)/He techniques to the samples from drill cores transecting the Lavanttal fault system, Eastern Alps. Apatite FT ages and lengths exhibit slight reductions toward the fault cores, whereas apatite (U–Th)/He ages also show younger ages in the fault cores. These results suggest that the samples were reheated either by frictional heating and/or by hot fluid flow within the fault zone.

Instead, illite K–Ar and $^{40}Ar/^{39}Ar$ analyses have widely been applied to date fault gouges under a variety of tectonic settings. The age of authigenic illite, formed in situ within the fault zone, should directly date the time of (some stages of) fault zone activity. After some pioneering studies, van der Pluijm and collaborators succeeded in quantifying the ratio of authigenic and detrital micas for individual clay size fractions by using quantitative X-ray analysis of clay grain-size populations (e.g. van der Pluijm et al. 2001, 2006; Solum et al. 2005; Haines and van der Pluijm 2008). In addition, Zwingmann and collaborators further demonstrated the applicability of illite K–Ar dating by analysing Alpine fault gouges (e.g., Zwingmann and Mancktelow 2004; Zwingmann et al. 2010b).

Pseudotachylytes Dating the glassy matrix of pseudotachylytes has been attempted by several studies, including $^{40}Ar/^{39}Ar$ thermochronology (Vredefort dome, South Africa, by Reimold et al. 1990; North Cascade Mountains, western USA, by Magloughlin et al. 2001; Alpine Fault, New Zealand, by Warr et al. 2003; More-Trondelag Fault, Central Norway, by Sherlock et al. 2004), glass FT thermochronology (Alpine Fault, New Zealand, by Seward and Sibson 1985) and Rb–Sr geochronology (Quetico and Rainy Lake-Seine River fault, western Superior Canadian Shield, by Peterman and Day 1989). As shown in those studies, constraining the ages of the glassy matrix of pseudotachylyte likely encountered three potential pitfalls: i.e. we do not know whether or not:

- Complete age resetting occurs as the result of frictional heating during pseudotachylyte formation. This is primarily an issue of diffusion kinetics of the radiogenic isotope during flash heating. In the case of $^{40}Ar/^{39}Ar$ thermochronology, however, the presence of inherited argon at crustal depths may further violate the key assumptions of dating pseudotachylyte, i.e. the host-rock

argon is lost to an infinite reservoir during near-instantaneous frictional melting (Sherlock et al. 2004).
- The isotopic system has been affected by later thermal events. Possible breakdown of the radiometric closed system is probably an issue of diffusion kinetics of the radiogenic isotope in hydrothermal heating environments, but could also be caused by devitrification of the glassy matrix of pseudotachylytes, as often observed in nature.
- The glassy matrix of the pseudotachylyte is completely free of pieces of country rock. If not, the complete resetting of the age will be extremely difficult for some of the thermochronologic techniques, such as $^{40}Ar/^{39}Ar$ method.

An alternative thermochronologic approach was adopted by Murakami and Tagami (2004), who carried out zircon FT analyses on a pseudotachylyte and its host rocks of the Nojima fault zone, southwest Japan (Fig. 12.3) (see Sect. 12.6.1). This new approach was subsequently applied to a variety of pseudotachylytes formed in different tectonic settings (e.g. Takagi et al. 2007, Tsergo Ri Landslide, Nepal; Takagi et al. 2010, Median Tectonic Line, southwest Japan). Both FT and U–Pb analyses were conducted on zircons separated from a pseudotachylyte layer and surrounding granitic fault rocks of the ancient Asuke shear zone, central Japan (Murakami et al. 2006a). The FT age of the pseudotachylyte is 53 ± 4 (1SE) Ma, which is significantly younger than the 73 ± 4 Ma age of the host rock away from the fault that gives the time of regional cooling. According to track-length information, the zircon FT data from the pseudotachylyte were interpreted to have been totally reset and subsequently cooled at ~53 Ma. Furthermore, U–Pb analysis shows a range of ages from ~67 to 76 Ma, which confirms that all of the host rocks formed approximately at the same time throughout the section.

Mylonites To constrain the time of ductile deformation in mylonites (Fig. 12.1a), application of the K–Ar (and $^{40}Ar/^{39}Ar$) systems to micas has predominantly been used in a variety of tectonic settings (e.g. Mulch et al. 2002; Sherlock et al. 2004; Rolland et al. 2007 and references therein). FT thermochronology has been applied to mylonites in ductile fault zones, as will be mentioned below, which may constrain steady-state heat generation by long-term faulting averaged over geological time (v = ~1–10 cm/year; see Sect. 12.2.3). In contrast to frictional heating at shallower depths within a brittle regime that generates short-term heat pulses, ductile deformation at deeper levels is characterised by long-term heating accompanied by a broader, regional thermal anomaly across the fault zone. This may result in regional metamorphic aureoles across convergent plate boundaries (or transcurrent shear zones) (Scholz 1980). In this regard, the Alpine fault, New Zealand, where the oblique convergence of two tectonic plates is ongoing (see Chap. 13, Baldwin et al. 2018), has been intensively studied by thermochronologic techniques. A systematic decrease in K–Ar ages over ~10 km was found toward the fault and was interpreted to represent an argon depletion aureole formed by long-term frictional heating at depth (Scholz et al. 1979, and references therein). This interpretation was based on a tectonic model suggesting that there was constant exhumation over the past 5 Myr throughout the study area. A later FT thermochronologic study, however, suggested the total amount of late Cenozoic exhumation exhibits an exponential increase toward the Alpine fault (Kamp et al. 1989). These authors estimated a differential, asymmetric uplift pattern across the fault, on the basis of apatite and zircon FT ages that show systematic trends to become younger toward the Alpine fault. They suggested that, as a result of the asymmetric exhumation, a 13–25 km wide regional metamorphic belt was exposed immediately to the east of the Alpine fault. More recent studies in the Southern Alps of New Zealand also interpreted the thermochronologic data in terms of exhumation (e.g., Little et al. 2005; Ring and Bernet 2010; Warren-Smith et al. 2016).

The Median Tectonic Line, southwest Japan, represents another example of long-term faulting that involves mylonite formation within a ductile regime. An apatite and zircon FT thermochronologic study was conducted on the granitic rocks of the Ryoke Belt, one of the regional metamorphic belts along the Median Tectonic Line (Tagami et al. 1988). A systematic age decrease of apatite FT ages over ~3–10 km toward the Median Tectonic Line was interpreted to be a consequence of long-term shear heating in the ductile fault zone. Recent FT and (U–Th)/He studies, however, have revealed regional differential exhumation histories of tectonic blocks that are bounded by neo-tectonic fault systems (Sueoka et al. 2012, 2016). Therefore, the previously observed age decrease toward the Median Tectonic Line may also be attributed to such differential uplift, rather than to a long-term shear heating process.

12.7 Summary and Future Perspectives

Fault zone rocks are the consequence of long-term, repeated motions of faults that reflect both spatial and temporal variations in tectonic stress regimes. Age determination of fault movements, therefore, plays a key role in understanding the geotectonics of faults and, particularly, in assessing the past seismic activity of an active fault system. The technical and methodological advancements of FT and other

thermochronological methods over the last few decades enable us to date a variety of fault zone materials formed during the development of a fault: e.g. (i) FT analysis of zircons from pseudotachylyte layers, fault gouge and associated deformed rocks, using the annealing kinetics based on the conventional laboratory heating experiments and also verified by flash and hydrothermal heating experiments; and (ii) K–Ar ($^{40}Ar/^{39}Ar$) dating on authigenic illite within a fault gouge, coupled with the evaluation of the influence of detrital contamination.

Furthermore, a series of drill cores into seismogenic fault zones, such as the Nojima Fault Zone Probe Project, offered the opportunity to systematically sample fresh fault zone rocks. These factors have provided a notable promotion of "fault zone thermochronology".

Further perspectives with respect to both the methodology and application of these techniques will be gained by:

- Additional laboratory flash and hydrothermal heatings as well as mechanical shearing experiments for a series of low-temperature thermochronological systems, such as apatite and zircon FT and (U–Th)/He, illite K–Ar ($^{40}Ar/^{39}Ar$) and quartz and feldspar ESR, TL and OSL systems. These will provide a more robust basis to interpret the fault zone thermochronologic data from a variety of fault zone rock types that represent different faulting depths and temperatures.
- A comparison of analysed data between thermochronologic methods having significantly different activation energies, such as zircon FT and (U–Th)/He. This may help to constrain the effective duration and temperature of fault zone thermal events, which will help to identify their heat source(s).
- A more systematically combined usage of apatite and zircon FT and (U–Th)/He, illite K–Ar, carbonate U–Th, and quartz and feldspar ESR, TL and OSL analyses on well-documented active fault systems, which will shed further light on our understanding of the thermomechanical processes in (paleo-) seismogenic-zone faults.

Acknowledgements The author thankfully acknowledges Ann Blythe and Meinert Rahn for their constructive and critical reviews of the manuscript, and Marco G. Malusà and Paul G. Fitzgerald for helpful editing of the chapter, particularly about the illustrations. The author thanks Masaki Murakami, Horst Zwingmann, Yumy Watanabe and Akito Tsutsumi for their helpful comments and arguments during the writing of the present chapter.

References

Ault AK, Reiners PW, Evans JP, Thomson SN (2015) Linking hematite (U–Th)/He dating with the microtextural record of seismicity in the Wasatch fault damage zone, Utah, USA. Geology 43:771–774

Baldwin SL, Fitzgerald PG, Malusà MG (2018) Chapter 13. Crustal exhumation of plutonic and metamorphic rocks: constraints from fission-track thermochronology. In: Malusà MG, Fitzgerald PG (eds) Fission-track thermochronology and its application to geology. Springer, Berlin

Boles JR, Eichhubl P, Garven G, Chen J (2004) Evolution of a hydrocarbon migration pathway along basin-bounding fault: evidence from fault cement. AAPG Bull 88:947–970

Boullier AM, Ohotani T, Fujimoto K, Ito H, Dubois M (2001) Fluid inclusions in pseudotachylytes from the Nojima fault, Japan. J Geophys Res 106:21965–21977

Brix MR, Stockhert B, Seidel E, Theye T, Thomson SN, Kuster M (2002) Thermobarometric data from a fossil zircon partial annealing zone in high pressure-low temperature rocks of eastern and central Crete, Greece. Tectonophysics 349:309–326

Brodsky EE, Mori J, Fulton PM (2010) Drilling into faults quickly after earthquakes. EOS Am Geophys Un 91:237–238

Carslaw HS, Jaeger JC (1959) Conduction of heat in solids. Oxford University Press, Oxford, 510 p

Cox SF (2005) Coupling between deformation, fluid pressures and fluid flow in ore-producing hydrothermal environments. In: Economic geology 100th anniversary volume, pp 39–75

Cox SF (2010) The application of failure mode diagrams for exploring the roles of fluid pressure and stress states in controlling styles of fracture-controlled permeability enhancement in faults and shear zones. Geofluids 10:217–233

d'Alessio MA, Blythe AE, Burgmann R (2003) No frictional heat along the San Gabriel Fault, California; evidence from fission-track thermochronology. Geology 31:541–544

Donelick RA, O'Sullivan PB, Ketcham RA (2005) Apatite fission-track analysis. Rev Mineral Geochem 58:49–94

Evans JP, Forster CB, Goddard JV (1997) Permeability of fault-related rocks, and implications for hydraulic structure of fault zone. J Struct Geol 19:1393–1404

Flotte N, Plagnes V, Sorel D, Benedicto A (2001) Attempt to date Pliestocene normal faults of the Corinth-Patras Rift (Greece) by U/Th method, and tectonic implications. Geophys Res Lett 28:3769–3772

Foster DA (2018) Chapter 11. Fission-track thermochronology in structural geology and tectonic studies. In: Malusà MG, Fitzgerald PG (eds) Fission-track thermochronology and its application to geology. Springer, Berlin

Fujimoto K, Ueda A, Ohtani T, Takahashi M, Ito H, Tanaka H, Boullier AM (2007) Borehole water and hydrologic model around the Nojima fault, SW Japan. Tectonophysics 443:174–182

Fukuchi T, Imai N (2001) ESR and ICP analyses of the DPRI 500 m drill core samples penetrating through the Nojima Fault, Japan. Isl Arc 10:465–478

Gallagher K (1995) Evolving temperature histories from apatite fission-track data. Earth Planet Sci Lett 136:421–435

Haines SH, van der Pluijm BA (2008) Clay quantification and Ar–Ar dating of synthetic and natural gouge: application to the Miocene Sierra Mazatan detachment fault, Sonora, Mexico. J Struct Geol 30:525–538

Holdsworth RE, Butler CA, Roberts AM (1997) The recognition of reactivation during continental deformation. J Geol Soc London 154:73–78

Kamp PJJ, Green PF, White SH (1989) Fission track analysis reveals character of collisional tectonics in New Zealand. Tectonics 8:169–195

Ketcham R (2018) Chapter 3. Fission track annealing: from geologic observations to thermal modeling. In: Malusà MG, Fitzgerald PG (eds) Fission-track thermochronology and its application to geology. Springer, Berlin

Lachenbruch H (1986) Simple models for the estimation and measurement of frictional heating by an earthquake. USGS Open File Rep 86-508

Little TA, Cox S, Vry JK, Batt G (2005) Variations in exhumation level and uplift rate along the oblique-slip Alpine fault, central Southern Alps, New Zealand. GSA Bull 117:707–723

Magloughlin JF, Hall CM, van der Pluijm BA (2001) ^{40}Ar–^{39}Ar geochronometry of pseudotachylytes by vacuum encapsulation: North Cascade Mountains, Washington, USA. Geology 29:51–54

Maino M, Casini L, Ceriani A, Decarlis A, Di Giulio A, Seno S, Setti M, Stuart FM (2015) Dating shallow thrusts with zircon (U–Th)/He thermochronometry—the shear heating connection. Geology 43:495–498

Malusà MG, Fitzgerald PG (2018) Chapter 8. From cooling to exhumation: setting the reference frame for the interpretation of thermocronologic data. In: Malusà MG, Fitzgerald PG (eds) Fission-track thermochronology and its application to geology. Springer, Berlin

Malusà MG, Fitzgerald PG (2018) Chapter 10. Application of thermochronology to geologic problems: bedrock and detrital approaches. In: Malusà MG, Fitzgerald PG (eds) Fission-track thermochronology and its application to geology. Springer, Berlin

Matsumoto H, Yamanaka C, Ikeya M (2001) ESR analysis of the Nojima fault gouge, Japan, from the DPRI 500 m borehole. Isl Arc 10:479–485

Metcalf JR, Fitzgerald PG, Baldwin SL, Munoz JA (2009) Thermochronology of a convergent orogeny: constraints on the timing of thrust faulting and subsequent exhumation of the Maladeta Pluton in the central Pyrenean axial zone. Earth Planet Sci Lett 287:488–503

Mulch A, Cosca MA, Handy MR (2002) In-situ UV-laser $^{40}Ar/^{39}Ar$ geochronology of a micaceous mylonite: an example of defect-enhanced argon loss. Contrib Mineral Petrol 142:738–752

Murakami M (2010) Average shear work estimation of Nojima fault from fission-track analytical data. Earth Monthly (in Japanese) 32:24–29

Murakami M, Tagami T (2004) Dating pseudotachylyte of the Nojima fault using the zircon fission-track method. Geophys Res Lett 31

Murakami M, Tagami T, Hasebe N (2002) Ancient thermal anomaly of an active fault system: zircon fission-track evidence from Nojima GSJ 750 m borehole samples. Geophys Res Lett 29

Murakami M, Kosler J, Takagi H, Tagami T (2006a) Dating pseudotachylyte of the Asuke Shear Zone using zircon fission-track and U–Pb methods. Tectonophysics 424:99–107

Murakami M, Yamada R, Tagami T (2006b) Short-term annealing characteristics of spontaneous fission tracks in zircon: a qualitative description. Chem Geol 227:214–222

Nuriel P, Rosenbaum G, Zhao JX, Feng Y, Golding SD, Villement B, Weinberger R (2012) U–Th dating of striated fault planes. Geology 40:647–650

O'Hara K (2004) Paleostress estimated on ancient seismogenic faults based on frictional heating of coal. Geophys Res Lett 31

Oshiman N, Ando M, Ito H, Ikeda R (eds) (2001) Geophysical probing of the Nojima fault zone. Isl Arc 10:197–198

Otsuki K, Monzawa N, Nagase T (2003) Fluidization and melting of fault gouge during seismic slip: identification in the Nojima fault zone and implications for focal earthquake mechanisms. J Geophys Res 108

Peterman ZE, Day W (1989) Early Proterozoic activity on Archean faults in the western Superior province—evidence from pseudotachylite. Geology 17:1089–1092

Reimold WU, Jessberger EK, Stephan T (1990) ^{40}Ar–^{39}Ar dating of pseudotachylite from the Vredefort dome, South Africa: a progress report. Tectonophysics 171:139–152

Ring U, Bernet M (2010) Fission-track analysis unravels the denudation history of the Bonar Range in the footwall of the Alpine fault, South Island, New Zealand. Geol Mag 147:801–813

Rolland Y, Corsini M, Rossi M, Cox SF, Pennacchioni G, Mancktelow N, Boullier AM (2007) Comment on "Alpine thermal and structural evolution of the highest external crystalline massif: The Mont Blanc" by P. H. Leloup, N. Arnaud, E. R. Sobel, and R. Lacassin. Tectonics 26

Scholz CH (1980) Shear heating and the state of stress on faults. J Geophys Res 85:6174–6184

Scholz CH (1988) The brittle-plastic transition and the depth of seismic faulting. Geol Runds 77:319–328

Scholz CH (2002) The mechanics of earthquakes and faulting, 2nd edn. Cambridge University Press, Cambridge, UK, 471 p

Scholz CH, Beavan J, Hanks TC (1979) Frictional metamorphism, argon depletion, and tectonic stress on the Alpine fault, New Zealand. J Geophys Res 84:6770–6782

Seront S, Wong TF, Caine JS, Forster CB, Bruhn RL, Fredrich JT (1998) Laboratory characterization of hydromechanical properties of a seismogenic normal fault system. J Struct Geol 20:865–881

Seward D, Sibson RH (1985) Fission-track age for a pseudotachylite from the Alpine fault zone, New Zealand. New Z J Geol Geophys 28:553–557

Sherlock SC, Watts LM, Holdsworth R, Roberts D (2004) Dating fault reactivation by Ar/Ar laserprobe: an alternative view of apparently cogenetic mylonite-pseudotachylite assemblages. J Geol Soc London 161:335–338

Shimamoto T, Takemura K, Fujimoto K, Tanaka H, Wibberley CAJ (2001) Nojima fault zone probing by core analyses. Isl Arc 10:357–359

Sibson RH (1975) Generation of pseudotachylite by ancient seismic faulting. Geophys J Royal Astron Soc 43:775–794

Sibson RH (1977) Fault rocks and fault mechanisms. J Geol Soc London 133:191–213

Sibson RH (1992) Implications of fault-valve behavior for rupture nucleation recurrence. Tectonophysics 211:283–293

Simpson C (1985) Deformation of granitic rocks across the brittle-ductile transition. J Struct Geol 5:503–512

Solum JG, van der Pluijm BA, Peacor DR (2005) Neocrystallization, fabrics, and age of clay minerals from an exposure of the Moab fault, Utah. J Struct Geol 27

Sueoka S, Kohn BP, Tagami T, Tsutsumi H, Hasebe N, Tamura A, Arai S (2012) Denudational history of the Kiso Range, central Japan, and its tectonic implications: constraints from low-temperature thermochronology. Isl Arc 21:32–52

Sueoka S, Tsutsumi H, Tagami T (2016) New approach to resolve the amount of Quaternary uplift and associated denudation of the mountain ranges in the Japanese Islands. Geosci Front 7:197–210

Tagami T (2005) Zircon fission-track thermochronology and applications to fault studies. Rev Mineral Geochem 58:95–122

Tagami T (2012) Thermochronological investigation of fault zones. Tectonophysics 538–540:67–85

Tagami T, Galbraith RF, Yamada R, Laslett GM (1998) Revised annealing kinetics of fission tracks in zircon and geological implications. In: van den Haute P, De Corte F (eds) Advances in fission-track geochronology. Kluwer, Dordrecht, The Netherlands, pp 99–112

Tagami T, Hasebe N, Kamohara H, Takemura K (2001) Thermal anomaly around Nojima fault as detected by the fission-track analysis of Ogura 500 m borehole samples. Isl Arc 10:457–464

Tagami T, Lal N, Sorkhabi RB, Nishimura S (1988) Fission track thermochronologic analysis of the Ryoke Belt and the Median Tectonic Line Southwest Japan. J Geophys Res 93:13705–13715

Tagami T, Murakami M (2007) Probing fault zone heterogeneity on the Nojima fault: constraints from zircon fission-track analysis of borehole samples. Tectonophysics 443:139–152

Tagami T, O'Sullivan PB (2005) Fundamentals of fission-track thermochronology. Rev Mineral Geochem 58:19–47

Takagi H, Arita K, Danhara T, Iwano H (2007) Timing of the Tsergo Ri Landslide, Langtang Himal, determined by fission track age for pseudotachylite. J Asian Earth Sci 29:466–472

Takagi H, Shimada K, Iwano H, Danhara T (2010) Oldest record of brittle deformation along the Median Tectonic Line: fission-track age for pseudotachylite in the Taki area, Mie Prefecture. J Geol Soc Japan 116:45–50

Tanaka H, Chester FM, Mori JJ, Wang CY (2007) Drilling into fault zones. Tectonophysics 443:123–125

van der Pluijm BA, Hall CM, Vrolijk PJ, Pevear DR, Covey MC (2001) The dating of shallow faults in the Earth's crust. Nature 412:172–175

van der Pluijm BA, Vrolijk PJ, Pevear DR, Hall CM, Solum J (2006) Fault dating in the Canadian Rocky Mountains: evidence for late Cretaceous and early Eocene orogenic pulses. Geology 34:837–840

Verhaert G, Muchez P, Sintubin M, Similox-Tohon D, Vandycke S, Keppens E, Hodge EJ, Richards DA (2004) Origin of paleofluids in a normal fault setting in the Aegean region. Geofluids 4:300–314

Viola G, Mancktelow NS, Seward D, Meier A, Martin S (2003) The Pejo fault system; an example of multiple tectonic activity in the Italian Eastern Alps. GSA Bull 115:515–532

Warr LN, van der Pluijm BA, Peacor DR, Hall CM (2003) Frictional melt pulses during a $\sim$1.1 Ma earthquake along the Alpine fault, New Zealand. Earth Planet Sci Lett 209:39–52

Warren-Smith E, Lamb S, Seward D, Smith E, Herman F, Stern T (2016) Thermochronological evidence of a low-angle, mid-crustal detachment plane beneath the central South Island, New Zealand. Geochem Geophys Geosyst 17:4212–4235

Watanabe Y, Nakai S, Lin A (2008) Attempt to determine U–Th ages of calcite veins in the Nojima fault zone, Japan. Geochem J 42:507–513

Wolfler A, Kurz W, Danisik M, Rabitsch R (2010) Dating of fault zone activity by apatite fission track and apatite (U–Th)/He thermochronometry: a case study from the Lavanttal fault system (Eastern Alps). Terra Nova 22:274–282

Yamada K, Hanamuro T, Tagami T, Shimada K, Takagi H, Yamada R, Umeda K (2012) The first (U–Th)/He dating of a pseudotachlylyte collected from the Median Tectonic Line, southwest Japan. J Asian Earth Sci 45:17–23

Yamada K, Tagami T, Shimobayashi N (2003) Experimental study on hydrothermal annealing of fission tracks in zircon. Chem Geol 201:351–357

Yamada R, Murakami M, Tagami T (2007) Statistical modelling of annealing kinetics of fission tracks in zircon; reassessment of laboratory experiments. Chem Geol 236:75–91

Yamada R, Tagami T, Nishimura S, Ito H (1995) Annealing kinetics of fission tracks in zircon: an experimental study. Chem Geol 122:249–258

Zwingmann H, Mancktelow N (2004) Timing of Alpine fault gouges. Earth Planet Sci Lett 223:415–425

Zwingmann H, Yamada K, Tagami T (2010a) Timing of brittle deformation within the Nojima fault zone, Japan. Chem Geol 275:176–185

Zwingmann H, Mancktelow N, Antognini M, Lucchini R (2010b) Dating of shallow faults: new constraints from the AlpTransit tunnel site (Switzerland). Geology 38:487–490